CrystEngComm

PAPER

View Article Online
View Journal

Cite this: DOI: 10.1039/d6ce00201c

Optimizing conditions for the formation of calcium oxalate trihydrate using the response surface methodology

Nives Matijaković Mlinarić, [a] Arijana Hamzić, [b] Nikolina Filipović, [b] Jelena Brdarić Kosanović, [b] Imre Szenti, [c] Marija Banožić [d] and Anamarija Stanković *[b]

Calcium oxalate (CaOx), the main component of kidney stones, occurs in several hydrated forms, among which calcium oxalate trihydrate (COT) is a rare and metastable phase believed to act as a transient precursor to the thermodynamically stable monohydrate. In this study, the response surface methodology (RSM), a statistical data analysis method that combines a specific experimental design with mathematical modeling, was applied to quantitatively evaluate and predict the influence of temperature, pH, and ionic strength on the formation of COT. The resulting precipitates were characterized using optical microscopy, scanning electron microscopy (SEM), Fourier-transform infrared spectroscopy (FTIR), and powder X-ray diffraction (PXRD). The results demonstrate that COT formation is favored at moderate temperatures, while higher temperatures promote the formation of calcium oxalate monohydrate (COM), whereas ionic strength exerts no significant effect under the investigated conditions. Overall, temperature was identified as the dominant parameter governing CaOx hydrate phase selection.

Received 11th March 2026,
Accepted 29th April 2026

DOI: 10.1039/d6ce00201c

rsc.li/crystengcomm

1. Introduction

The main goal of this study was to examine how key process parameters, specifically temperature, pH, and ionic strength shape the crystallization behavior of calcium oxalate hydrates. By systematically adjusting these conditions, we evaluated both their individual effects and their mutual interactions on the resulting crystal phases and morphologies. Using the response surface methodology (RSM), we identified conditions that favor the formation of two dominant hydrates: calcium oxalate monohydrate (COM) and trihydrate (COT). Detailed morphological and chemical analyses of the obtained crystals provided deeper insight into the circumstances that promote specific hydrate forms and the ways in which physicochemical parameters govern their growth and structural evolution.

Biomineralization is a widespread, natural process through which living organisms control the formation of inorganic minerals. This ability emerged early in Earth's history, around 3.5 billion years ago, as organisms developed genetically regulated mineralization pathways that support metabolic functions and facilitate adaptation to environmental stressors.[1–3] Although biomineralization varies across species, it is guided by shared principles such as the involvement of biomacromolecules, spatially regulated nucleation, and the frequent use of precursor phases. In healthy systems, mineral deposition is carefully controlled, occurring only at specific physiological sites while being suppressed in soft tissues such as the cardiovascular system. Pathological mineralization, on the other hand, arises when minerals form in tissues that do not normally calcify. This can occur in disease, during injury, inflammation, or with aging. Despite being less extensively investigated, pathological and physiological mineralization share important mechanistic features, and many aspects including mineral composition, cellular participation, and regulatory pathways remain subjects of active research.[4–6] Kidney stones are typically composed of approximately 90% mineral material and 10% organic components. The mineral portion includes calcium-based stones such as calcium oxalate (CaOx) and calcium phosphate (CaP), as well as non-calcium stones including struvite, uric acid, cystine, proteinaceous stones, and those formed through pharmaceutical crystallization.[7] Most stones are heterogeneous in composition; for mixed calculi, roughly 80% contain varying

[a] Ruđer Bošković Institute, Bijenička cesta 54, 10000 Zagreb, Croatia. E-mail: nives.matijakovic@irb.hr
[b] Department of Chemistry, University of Osijek, Ulica cara Hadrijana 8/A, 31000 Osijek, Croatia. E-mail: arijanahamzic1@gmail.com, nfilipovic@kemija.unios.hr, jbrdaric@kemija.unios.hr, astankovic@kemija.unios.hr, ster.anamarija@gmail.com
[c] Department of Applied and Environmental Chemistry, University of Szeged, Rerich Béla tér 1, H-6720 Szeged, Hungary. E-mail: szentiimre@gmail.com
[d] Faculty of Agriculture and Food Technology, University of Mostar, Biskupa Čule bb, 88000 Mostar, Bosnia and Herzegovina. E-mail: marija.banozic@aptf.sum.ba

proportions of CaOx and CaP, while stones consisting of a single, unusual compound are relatively uncommon.[8] Kidney stones affect between 1.7% and 14.8% of people at least once in their lifetime, and recurrence within five years is estimated at around 40%. Calcium oxalate stones dominate, representing more than 80% of diagnosed cases. Supersaturation of urinary calcium oxalate is the major driving force behind stone formation, highlighting the importance of understanding crystallization mechanisms and the potential of inhibitors in preventive strategies.[9,10] Calcium oxalate occurs in four pseudo-polymorphic forms: the anhydrous phase, calcium oxalate monohydrate (COM, whewellite), calcium oxalate dihydrate (COD, weddellite), and calcium oxalate trihydrate (COT, caoxite).[11] COM and COD are the most frequently encountered phases in kidney stones, whereas COT appears only occasionally.[12] In urine, COM is the thermodynamically stable phase, while COD is metastable and exhibits higher solubility.[13,14] Caoxite, like COM, is associated with hyperoxaluric conditions, but its rare occurrence suggests the involvement of additional factors that influence its formation.[15–17] Thermodynamically, COT is highly unstable and undergoes spontaneous transformation to COM within hours under *in vitro* conditions.[18] Therefore, its detection in urinary calculi implies that specific urinary environments may temporarily stabilize this otherwise transient phase. In most reported cases, COT appears alongside COM, indicating that its rapid transformation complicates the clinical observation of a pure COT phase. Previous studies have shown that CaOx phase formation is primarily governed by pH and supersaturation, while temperature is often held constant and ionic strength is implicitly defined by solution composition.[19] High supersaturation and elevated pH favor the formation of metastable hydrates such as COD and, in rarer cases, COT. In contrast, low pH, lower supersaturation, and prolonged ageing promote the formation of the thermodynamically stable COM. Crystal size, morphology, and phase distribution are strongly influenced by these variables as well as by external energy input.[20] These findings highlight the need for careful control of physicochemical parameters when studying CaOx crystallization. Metastable dihydrate phases like COD and COT can act as precursors to COM, and their transformation is influenced by temperature, pH, and ionic composition. Understanding these transitions is essential, as they affect crystal morphology and potential clinical behavior.[16,17] Calcium oxalate crystallization predominantly yields COM and COD, with their stability shaped by environmental conditions.[20–22] Temperature plays a particularly significant role, as COD converts to COM in aqueous media at 37 °C through well-defined kinetic pathways.[23] Many experiments have been conducted at a fixed pH of around 6, indicating the importance of pH in CaOx precipitation, although its specific contributions have not always been studied systematically. Ionic composition further affects phase stability, as crystallization inhibitors, such as citrate and pyrophosphate, can stabilize COD and slow its conversion to COM by interacting with calcium ions and specific crystal planes. Hydration processes also contribute: COD contains weakly bound zeolitic water that can be exchanged with the surrounding medium, triggering structural rearrangements that lead to the formation of COM.[20,24–27] Together, these observations underscore the combined importance of temperature, hydration state, and ionic interactions in determining CaOx phase behavior. Both thermodynamic and kinetic factors influence the inhibition of CaOx crystallization. Hydroxycitrate reduces supersaturation by binding free calcium ions, a thermodynamic mechanism, whereas phytate slows nucleation and crystal growth by binding to crystal surfaces, representing a kinetic effect. Combining inhibitors with complementary mechanisms may therefore enhance overall suppression of stone formation.[28] Understanding how calcium oxalate phases form and transform is vital for interpreting their presence in both biological and environmental aqueous systems. Detailed structural and mechanistic investigations provide insights into the stability relationships between different hydrates and the pathways by which they interconvert. Such knowledge is essential for identifying the physicochemical conditions that govern nucleation, growth, and transformation, ultimately improving our ability to predict CaOx behavior under diverse aqueous conditions.

Despite notable progress, significant knowledge gaps remain. Many studies focus on isolated parameters under well-controlled laboratory conditions, whereas the combined effects of temperature, ionic strength, and solution composition have been far less systematically explored. In particular, the simultaneous influence of temperature and ionic strength on CaOx formation, and their interplay with organic components and complexing ligands, including implications for COT stability remains insufficiently understood. Addressing these gaps is essential for bridging the divide between controlled laboratory experiments and real aqueous environments, where multiple parameters interact to govern calcium oxalate phase behavior.

In this context, the present study employs the response surface methodology (RSM) to systematically evaluate the combined effects of key physicochemical parameters and to identify conditions that enable the formation of calcium oxalate trihydrate (COT). Importantly, this approach allows for the targeted synthesis of phase-pure COT without the use of additives, distinguishing it from the majority of previously reported systems and providing a clearer framework for understanding intrinsic formation pathways.

2. Materials and methods

2.1. Materials

All chemicals used in this study were of analytical grade. The stock solutions for precipitation experiments were prepared using hydrochloric acid (HCl) and sodium hydroxide (NaOH) obtained from Gram-mol, sodium oxalate ($Na_2C_2O_4$) and

calcium chloride dihydrate ($CaCl_2 \times 2H_2O$) from BDH Prolabo, and sodium chloride (NaCl) from Kemika. Working solutions of calcium ions were prepared by diluting a $CaCl_2$ stock solution with ultrapure deionized water (conductivity < 0.055 μS cm^{-1}). Oxalate ion solutions were freshly prepared for each experiment by accurately weighing solid $Na_2C_2O_4$ and dissolving it in ultrapure deionized water to achieve the desired concentration. The controlled addition of NaOH or HCl stock solutions adjusted the pH of the reaction system. All stock solutions were standardized using conventional analytical techniques: $CaCl_2$ was standardized by complexometric titration with EDTA, and standard solutions of NaOH and HCl were also standardized accordingly.

2.2. Precipitation experiments

The experimental synthesis of calcium oxalate was based on a spontaneous precipitation approach with modifications applied to previously established protocols.[29–33] Each reaction system contained predefined concentrations of calcium (Ca^{2+}, 4.0×10^{-3} mol dm^{-3}) and oxalate ions ($C_2O_4^{2-}$, 0.7×10^{-3} mol dm^{-3}). The pH values of the solutions were adjusted to fall within the range of 5.6 to 7.5. Precipitation experiments were conducted at three controlled temperatures: 25 °C, 36.5 °C, and 48 °C. Reactions were carried out in a double-jacketed glass reactor connected to a thermostatic water bath to maintain constant temperature. Prior to mixing, the individual calcium and oxalate solutions were equilibrated to the target temperature and adjusted to the desired pH. The reaction was initiated by rapidly combining equal volumes (200 cm^3) of the two solutions under constant stirring using a Teflon-coated magnetic stir bar. The progress of the reaction was monitored in real time using a combined glass electrode connected to a digital pH meter (HANNA HI 5522), which recorded pH changes throughout the process (pH *vs.* time). Stirring continued for 45 minutes to allow sufficient time for crystal formation. At the end of the experiment, the suspension was filtered using a 0.22 μm Millipore membrane filter. The collected solids were rinsed with small volumes of deionized water and then dried in a vacuum desiccator. All experiments were conducted in triplicate to ensure reproducibility, and average values are reported in the results.

2.3. Data analysis

The initial supersaturations of the precipitation systems were calculated using Visual MINTEQ 3.1 software (freely available at https://vminteq.com/). Supersaturation was expressed as the saturation ratio, S, defined as the square root of the quotient of the ion activity product, $\Pi = a(Ca^{2+}) \cdot a(C_2O_4^{2-})$ and the thermodynamic equilibrium constant, K^0_{sp} for calcium oxalate monohydrate (COM) or trihydrate (COT): $S_{COM\ or\ COT} = (\Pi/K^0_{sp})^{1/2}$.

The calculations accounted for the initial reactant concentrations (c_i), temperature (t), and initial pH. To maintain a constant ionic strength (I_c), NaCl was added to the systems according to the values obtained from the VMINTEQ simulations. As shown in Table S1, the calculated initial saturation ratios for COM ranged from 11.228 ± 1.970, while for COT, the values were 6.799 ± 1.246. Under the given experimental conditions, the initial supersaturation in all systems can be characterized as moderate to high. Given the nature of the precipitation process, the variations in values across different systems were considered minor, allowing the supersaturation to be treated as nearly uniform across all experiments.

2.4. Sample characterization

To identify the hydrate phase and determine the mineralogical composition of the synthesized calcium oxalate crystals, a combination of analytical techniques was employed, including powder X-ray diffraction (PXRD), Fourier-transform infrared spectroscopy (FTIR), and microscopy. Fourier-transform infrared spectroscopy was used to analyze the vibrational characteristics of the crystal structures. Approximately 1–3 mg of each dried sample was homogenized with IR-grade potassium bromide (KBr). Spectra were recorded using an FTIR 8400S spectrophotometer (Shimadzu, Kyoto, Japan) over the spectral range of 400–4000 cm^{-1}. Each spectrum represents the average of 20 scans, acquired at a spectral resolution of 4 cm^{-1}. The instrument was equipped with a DRS 8000 diffuse reflectance accessory, and data processing was performed using the IRsolution 1.30 software package. Powder X-ray diffraction patterns were obtained using a PANalytical Aeris diffractometer (Malvern PANalytical, UK) with Cu Kα radiation (λ = 1.5418 Å), operated at 40 kV and 15 mA. Data were collected in the 2θ range of 10–60°, with a step size of 0.02° and a 1° divergence slit. Phase identification was conducted by matching the diffraction patterns to entries in the Crystallography Open Database (COD), and quantitative phase analysis was carried out using Rietveld refinement with HighScore Plus software (version 3.0). Crystal morphology and approximate particle size were examined using both optical and scanning electron microscopy. Optical observations were performed with a Motic B1 light microscope (Barcelona, Spain) equipped with a Moticam 2 digital camera. Scanning electron microscopy (SEM) was conducted using a Thermo Fisher Scientific Apreo C SEM system (Waltham, MA, USA). For SEM imaging, a small amount of sample was mounted on aluminum stubs using carbon adhesive tape. Loose particles were removed by a gentle nitrogen gas flow to minimize background interference.

2.5. Response surface methodology and process optimization in calcium oxalate formation

To determine the optimal conditions for maximizing the formation of specific calcium oxalate hydrate phases (COM and COT), the response surface methodology (RSM) was applied using a Box–Behnken experimental design. Statistical

modeling and analysis were carried out using the Design-Expert® software (version 9, Stat-Ease Inc., Minneapolis, MN, USA).

The relationships between the experimental variables, temperature (X_1), pH (X_2), and ionic strength (X_3), and the resulting content of individual hydrate phases, were evaluated by fitting second-order polynomial models (quadratic form) to the experimental data. No data transformation was applied during model fitting. The adequacy and significance of the models were assessed through analysis of variance (ANOVA).

The general form of the regression model used is represented by eqn (1):

$$y = \beta_0 + \sum_{i=1}^{k} \beta_i X_i + \sum_{i=1}^{k} \beta_{ii} X_i^2 + \sum_{\substack{i=1 \\ i<j}}^{k-1} \sum_{j=2}^{k} \beta_{ij} X_i X_j \quad (1)$$

where y represents the predicted response (the relative content of COM or COT), β_0 is the intercept term, β_i, β_{ii}, and β_{ij} are the coefficients corresponding to linear, quadratic, and interaction effects, respectively, and X_i and X_j denote the coded levels (−1, 0, +1) of the independent variables (as defined in Table 1).

This modeling approach enabled both the evaluation of individual factor effects and their interactions, as well as the identification of optimal experimental conditions for enhancing the yield of the desired hydrate phase.

3. Results and discussion

3.1. Structural analysis

Table 2 summarizes the experimental conditions, each labelled as a separate 'Run'. For clarity and to enhance the presentation of results, a selection of representative runs (specifically runs 1, 3, 9, 11, and 13) was chosen for detailed discussion.

In this work, FTIR spectroscopy was used primarily as a qualitative analytical technique to identify and distinguish between the hydrate phases of calcium oxalate. The FTIR spectra of samples (run 1, run 3, run 9, run 11, and run 13 (Fig. 1)) provide clear evidence for the presence of COT and COM (Table S2). The samples identified as pure COT (run 1, run 9 and run 13) exhibit FTIR features characteristic of trihydrate structures (Fig. 1), primarily manifested in the broad and complex O–H stretching region between 3600 cm^{-1} and 3000 cm^{-1}. This complexity arises from the presence of three crystallographically distinct water molecules in COT, each involved in different hydrogen-bonding interactions, as previously described by Conti *et al.*,[34] who emphasized the role of multiple hydrogen-bonding environments in shaping the vibrational profile of caoxite (COT). Furthermore, the enhanced splitting of bands in the 1600–1300 cm^{-1} region, corresponding to the asymmetric and symmetric stretching modes of the oxalate group, as well as the presence of multiple bands in the

Table 1 RSM design using the uncoded and coded levels of independent variables for the preparation of individual calcium oxalate hydrate phases (dependent variable; *y*)

		Level		
Independent variable	Symbol	Low (−1)	Center (0)	High (+1)
Temperature (°C)	X_1	25	36.5	48
System pH	X_2	5.60	6.55	7.50
Ionic strength (mol dm^{-3})	X_3	0.01	0.05	0.10

Table 2 Box–Behnken experimental design and identification of calcium oxalate hydrate phases by XRD analysis (response variables, *y*, quantified by XRD). Samples selected for detailed characterization are highlighted in bold. The experimental error for phase quantification was determined by calculating the standard deviation (SD) of the five center point replicates (runs 1, 6, 7, 10, and 16). The calculated SD is 0.26 for COT and COM, respectively

	Operating parameters			Response	
	Temperature		Ionic strength	COT	COM
Run	°C	System pH	mol dm^{-3}	%	
1	**36.5**	**6.55**	**0.055**	**100**	**0**
2	36.5	5.60	0.01	44.6	55.4
3	**36.5**	**5.60**	**0.1**	**41.2**	**58.8**
4	36.5	7.50	0.1	100	0
5	48.0	5.60	0.055	0	100
6	36.5	6.55	0.055	99.4	0.6
7	36.5	6.55	0.055	100	0
8	48.0	6.55	0.01	0	100
9	**25.0**	**6.55**	**0.1**	**100**	**0**
10	36.5	6.55	0.055	100	0
11	**48.0**	**6.55**	**0.1**	**0**	**100**
12	48.0	7.5	0.055	0	100
13	**25.0**	**7.5**	**0.055**	**100**	**0**
14	36.5	7.5	0.01	98.8	0.2
15	25.0	6.55	0.01	98.8	0.2
16	36.5	6.55	0.055	100	0
17	25.0	5.6	0.055	100	0

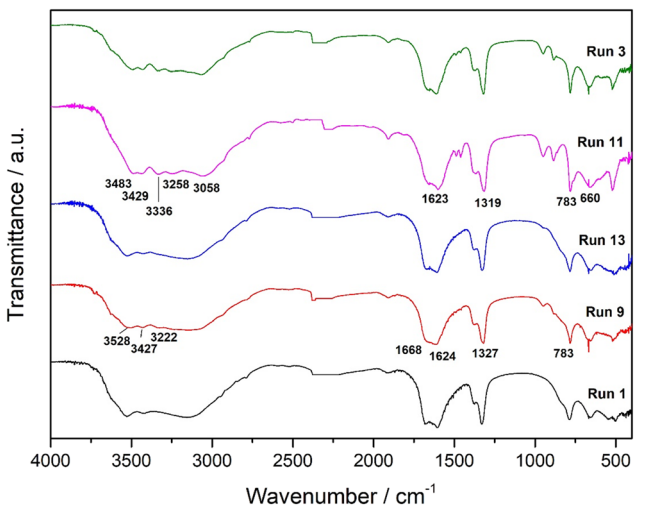

Fig. 1 FTIR spectra of precipitated systems: run 1, run 9, run 13, run 11, and run 3. Some standard vibration bands of COT (run 9) and COM (run 11) are indicated for comparison.

fingerprint region between 800 cm^{-1} and 600 cm^{-1}, aligns well with the vibrational assignments published for calcium oxalate trihydrate.[34] In contrast, run 11, identified as pure COM, demonstrates a distinctly different FTIR pattern. The O–H stretching region showed five peaks above 3000 cm^{-1}, in agreement with the presence of a single structural water molecule in whewellite (COM). The characteristic strong band near 1620 cm^{-1} observed in run 11 corresponds to the $\nu_{as}(COO^{-})$ mode typical of COM, while the sharp and intense absorption around 783 cm^{-1} represents a key diagnostic feature that has been widely used to distinguish COM from other hydrates. These spectral features confirm the high phase purity of the COM sample.[14,35] The spectrum of run 3 displays a combination of both COM and COT vibrational features, confirming that this sample contains a mixture of monohydrate and trihydrate phases. The overlap of the broad O–H stretching bands (typical for COT) with the more defined COM absorptions, particularly the 783 cm^{-1} peak, provides strong evidence for coexistence of the two hydrate forms.[36] FTIR was employed for qualitative analysis in this research.

The PXRD diffraction patterns obtained for the synthesized samples (run 1, run 3, run 9, run 11 and run 13) presented in Fig. 2 confirm the phase composition inferred from FTIR and provide additional structural evidence for identifying COT and COM. The reference diffractograms for pure COT and COM (included at the bottom of Fig. 2) allow direct comparison of peak positions and relative intensities, enabling unambiguous phase identification. The samples (run 1, run 9 and run 13) exhibit diffraction patterns that match those of pure COT.[22] Run 11, in contrast, shows diffraction maxima fully consistent with COM.[22,32,36] COM is known to crystallize in a monoclinic lattice, producing a sharper and simpler diffraction pattern with well-defined dominant reflections. These structural features are in line with previous detailed analyses reported by Petit *et al.*, who highlighted the differences in lattice geometry and hydration degree that distinguish COM from higher hydrates.[36] The most notable case is run 3, for which Rietveld refinement indicates a biphasic composition consisting of 41% COT and 58% COM. The phase composition (wt%) of calcium oxalate hydrates and the corresponding Rietveld refinement indicators (R_e, R_p, R_{wp}, GoF) for each experimental run are presented in Table S3. This quantitative result aligns closely with the corresponding diffraction pattern, which shows peak sets attributable to both hydrates. The presence of reflection groups characteristic of COM superimposed with the broader and more numerous reflections characteristic of COT confirms the mixed nature of the sample.

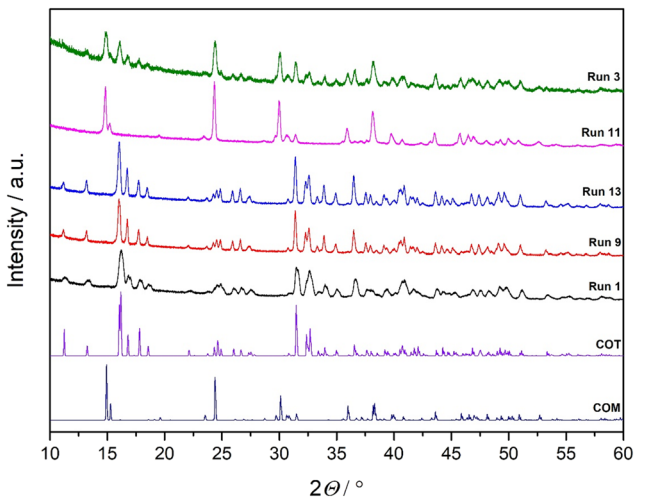

Fig. 2 PXRD diffraction patterns of precipitated systems: run 1, run 9, run 13, run 11, and run 3. Standard diffraction spectra of COT and COM are shown for comparison.

3.2. Morphology of calcium oxalate crystals

The morphology and size of the synthesized crystallites were characterized using a light microscope (Fig. S1) and SEM. SEM images of selected samples are presented in Fig. 3 (run 1 – A, run 9 – B, run 13 – C, run 11 – D, and run 3 – E). In the images where only COT precipitated (Fig. 3: A, B, and C), the COT crystals appear relatively large and exhibit an elongated, sword-like morphology.[37,38] In Fig. 3E, smaller and more aggregated COM crystals are observed on the surface of COT crystals. Additionally, some COT crystals display a hexagonal squat shape.[38] COM crystals are mostly irregular in shape, with noticeable aggregation and formation of larger clusters. In Fig. 3D, well-defined COM crystals are visible, exhibiting the characteristic boat/coffin or elongated hexagonal morphology previously reported in the literature.[38,39] Significant aggregation and intergrowth of COM crystals are also evident. It can be observed that the crystals in Fig. 3D and E are considerably smaller compared to those in Fig. 3A–C. The morphological characteristics identified are in good agreement with results obtained by other methodological approaches.

Although Fig. 3 shows the morphologies of COT crystals at positions A, B, and C, the higher-magnification SEM image in Fig. 4 reveals that differences in the crystal surface are present.

The differences observed in the surface morphology of the COT crystals likely arise from variations in synthesis conditions. Fig. 4A (run 1) shows that higher temperature (36.5 °C) promotes more uniform crystal growth and results in smoother crystal surfaces, consistent with findings by Tomazic and Nancollas,[40] who reported that the growth and transformation of COT are highly sensitive to temperature and ionic strength. Fig. 4B (run 9) shows that elevated ionic strength (0.10 mol dm^{-3}) leads to an increase in surface defects and cracking. Fig. 4C (run 13) shows that higher pH (7.5) can alter the relative stability of hydrated phases and produce heterogeneous, lamellar structures, which agrees with biomimetic studies by Thomas *et al.*[41]

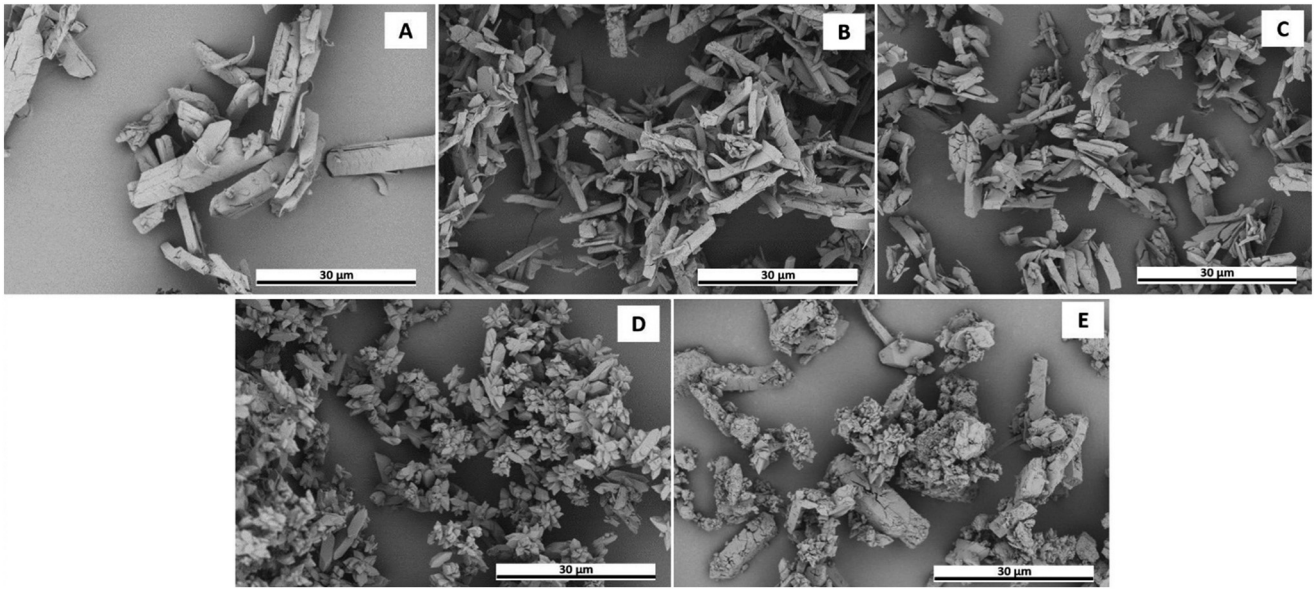

Fig. 3 Scanning electron microscopy images illustrating the morphological diversity of calcium oxalate crystals obtained in different experimental runs: (A) run 1, (B) run 9, (C) run 13, (D) run 11, and (E) run 3.

3.3. Modeling and optimization of process parameters influencing calcium oxalate hydrate phase formation

The 3-factor independent quadratic Box–Behnken design (BBD), and the predicted data and results obtained through 17 experiments for the formation of calcium oxalate hydrates are presented in Table 2. The COT ranges between (0–100)% and (−14.10–114.10)% for the experimental and predicted responses. The predicted response values slightly exceeding the theoretical range (0–100%) are a consequence of the mathematical nature of the quadratic polynomial regression model. These values represent an extrapolation by the model to fit the overall curvature of the response surface. For physical interpretation and optimization purposes, predicted values below 0% or above 100% are treated as 0% and 100%, respectively, representing the absolute phase purity boundaries. The BBD was employed to develop a quadratic polynomial regression model (eqn (1) and (2)) where X_1 represents temperature, X_2 pH and X_3 ionic strength. The given equations represent an empirical relationship between COM and COT content as dependent variables and formation condition as independent variables. Significance of the model equation was determined using the analysis of variance (ANOVA) and F-test (Fisher's test) (Table S4). Notably, all examined variables influencing COM production were found to be statistically significant (p-value < 0.05), with an overall significant model and a non-significant lack of fit (Table S4). The resulting coefficient of determination was $R^2 = 0.9402$. Likewise, the adequacy of the model for COT determination was confirmed by p-values below 0.05, indicating statistical significance, along with a non-significant lack of fit (p-value > 0.05) (Table S4). All input variables were significant in this case as well, with an obtained value of $R^2 = 0.9372$. The findings indicate that the data correspond to a quadratic model, represented by the following coded equations for COT (2) and COM (3):

$$\mathrm{COT} = 96.4 - 4.85X_1 + 14.25X_2 - 0.25X_3 - 34.05{X_1}^2 - 12.35{X_2}^2 - 12.65{X_3}^2 \quad (2)$$

$$\mathrm{COM} = 3 + 49.97X_1 + 14.25X_2 - 0.375X_3 - 34.22{X_1}^2 - 12.77{X_2}^2 - 12.83{X_3}^2 \quad (3)$$

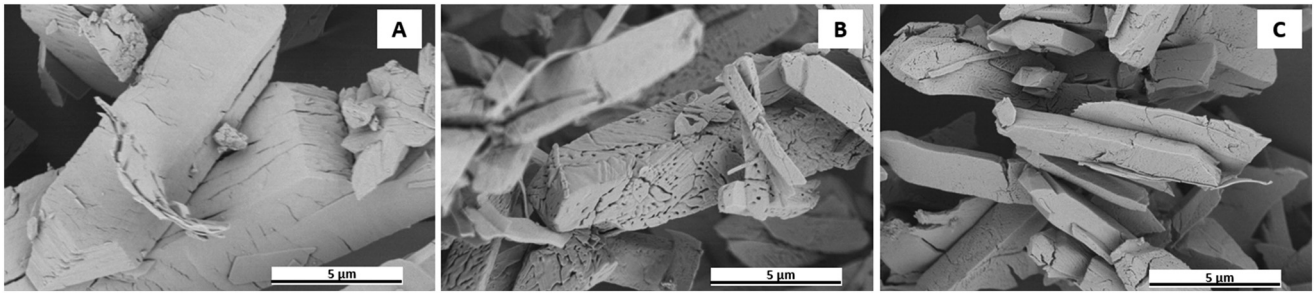

Fig. 4 Higher-magnification SEM images illustrating the morphological diversity of COT obtained in experimental runs: (A) run 1, (B) run 9 and (C) run 13.

Three influencing factors, namely temperature, pH value and ionic strength, were combined in the BBD to minimize the number of experimental runs and to examine the effect of selected parameters and their interaction on COM and COT creation.

The response surface regression results are given in Table S5. The table provides coefficients along with their standard error, F and p-values. The p-value presents the smallest level of significance, which could lead to the rejection of a null hypothesis. According to Table S5, the linear coefficients of temperature and pH value, and quadratic coefficient of temperature had a significant effect ($p \leq 0.05$) on COM and COT yield. The RSM analysis results revealed that the lower temperature, ionic strength and higher pH values promoted high COT content, while the opposite was observed for COM values. In contrast, the quadratic coefficients had a negative effect on COT yield and a positive effect on COM yield. This indicates that, for example, the COT yield initially increases as temperature increases, reaches a maximum within the experimental range, and then begins to decrease. As shown in Fig. 5A and B (and Fig. S2A), COT precipitates at a 100% yield between 25 °C and 36.5 °C. However, further increases in temperature within the experimental range (up to 48 °C) result in a pronounced decrease in COT yield. The effects of

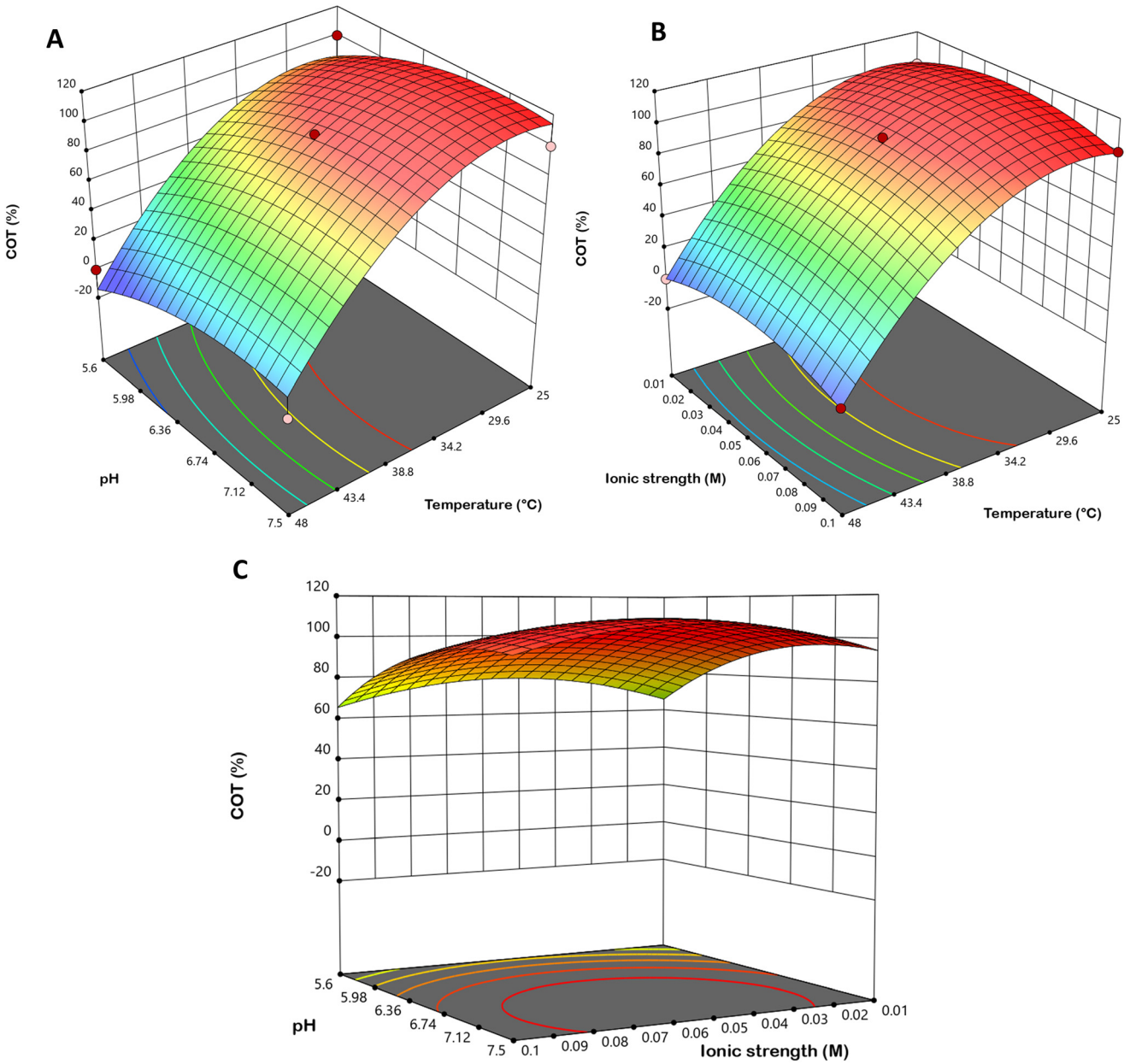

Fig. 5 3D plots of the influence of individual parameters and their interactions: (A) temperature (X_1) and system pH (X_2), (B) temperature (X_1) and ionic strength (X_3), and (C) system pH (X_2) and ionic strength (X_3) on the COT content response (y), derived from quantitative phase analysis of XRD data used as input for the RSM model.

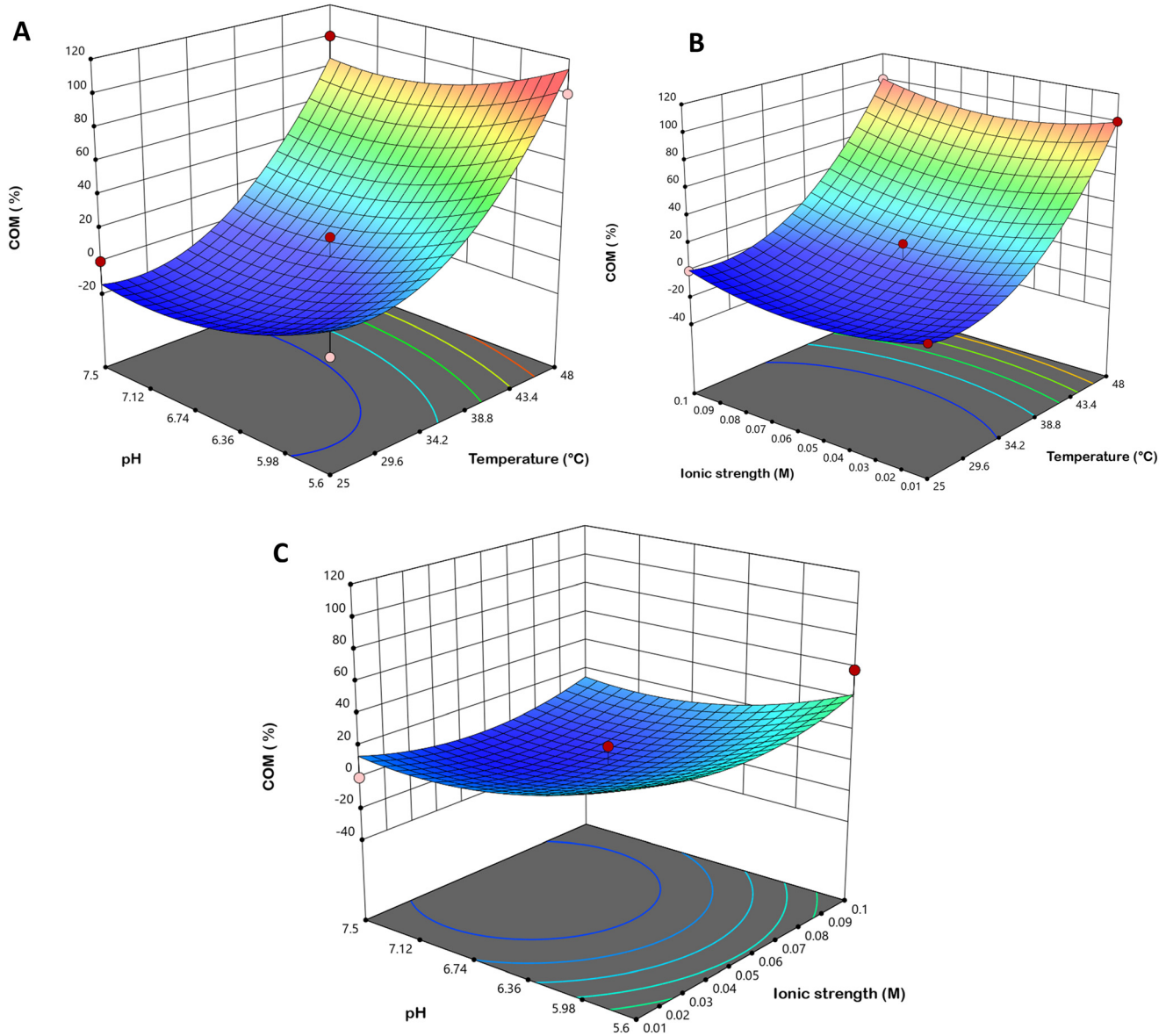

Fig. 6 3D plots of the influence of individual parameters and their interactions: (A) temperature (X_1) and system pH (X_2), (B) temperature (X_1) and ionic strength (X_3), and (C) system pH (X_2) and ionic strength (X_3) on the COM content response (y), based on quantitative phase fractions obtained from XRD analysis.

pH (Fig. 5A and C and S2A) and ionic strength (Fig. 5B and C and S2A) demonstrate that a pH above 6.36 consistently leads to COT precipitation. The ionic strength in all experiments was maintained between 0.01 mol dm^{-3} and 0.10 mol dm^{-3}, which is generally considered low. Thus, it may be concluded that, under the investigated conditions, the tested ionic strength does not exert any appreciable influence on COT precipitation.

Similarly, as illustrated in Fig. 6, the COM yield increases gradually between 25 °C and 38 °C, followed by a pronounced rise above 34 °C as the temperature continues to increase. The effects of pH (Fig. 6A and C and S2A) and ionic strength (Fig. 6B and C and S2A) show that COM precipitation occurs at pH values below 6.5. Furthermore, as observed for COT precipitation, the ionic strength did not exhibit any notable influence on COM formation.

The statistical robustness of the proposed models is reflected in the R^2 and values, which were 0.9372 and 0.8995 for COT, and 0.9402 and 0.9043 for COM, respectively. These values suggest an acceptable goodness-of-fit, with predicted and experimental data showing a clear, strong correlation. The resulting fitting eqn (2) and (3) successfully described the dependence of hydrate yields on the independent variables (R^2_{adj}, pH and ionic strength). By applying a desirability function approach to maximize COT yield while minimizing COM formation, the optimal conditions (Table 3) were determined to be 34.25 °C, pH 7.35 and I_c = 0.093 mol dm^{-3}. The experimental verification of these conditions

Table 3 Optimal conditions for COT synthesis

Optimal conditions			Predicted COT value (%)	Obtained COT value (%)	Predicted COM value (%)	Obtained COM value (%)
Temperature (°C)	System pH	Ionic strength (mol dm^{-3})				
34.25	7.35	0.093	98.91	100	1.00	0

yielded results within a 5% deviation from the theoretical predictions, confirming that the models are highly predictive for the COT formation process. Given that the mechanisms for COM formation are well-established in the literature, the subsequent discussion focuses exclusively on the factors governing the formation and stabilization of COT.

The characterization of the COT crystals obtained under optimal experimental conditions is presented in Fig. 7. A representative microscopy image (Fig. 7A) provides an initial overview of the crystal morphology at 10× magnification. To confirm the phase purity (Fig. S3 and Table S6), XRD analysis was performed (Fig. 7B). The diffraction pattern of the optimized sample (black line) shows excellent agreement with the standard COT reference spectra (red line). Further detailed morphological insights were obtained through SEM, as shown in Fig. 7C and D.

The influence of temperature observed in this study aligns with previous findings where higher crystallization temperatures typically favor the more thermodynamically stable COM, while lower temperatures increase the proportion of hydrated phases like COT or COD.[32,42,43] Specifically, we observed that while a slight increase from 25 °C to 27 °C may enhance COT yield, further increases up to 48 °C lead to a significant decline. This temperature dependence is closely linked to the kinetic window of metastable phases. As demonstrated by Brečević and Kralj,[44] COT preferentially forms under kinetically controlled conditions, particularly at moderate temperatures around 25 °C, and no longer appears in precipitates above 37 °C. Our experimental window (25–36.5 °C) and relatively short reaction time of 45 minutes were precisely situated to favor COT nucleation while preventing its rapid conversion into

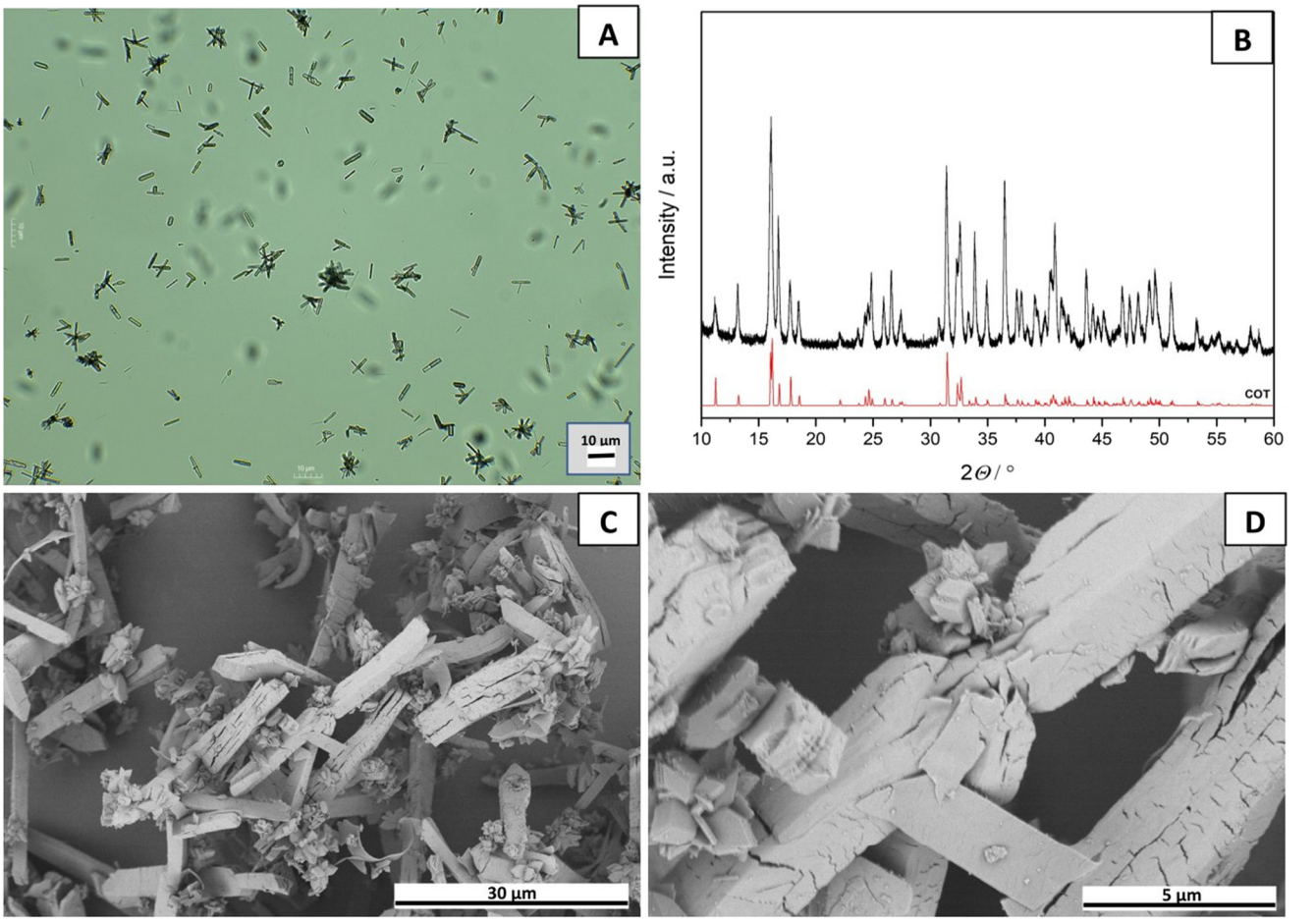

Fig. 7 COT obtained under optimal conditions; (A) microscopy image (×10), (B) XRD diffraction patterns of the optimized sample for COT (black) and standard diffraction spectra of COT (red), (C) and (D) SEM images.

the more stable COM.[45] The strong influence of temperature suggests that COT formation is kinetically driven rather than thermodynamically favored. Higher temperatures increase ion mobility and supersaturation dynamics, potentially promoting rapid nucleation of less stable hydrated phases before transformation to more stable forms such as COM. This supports the hypothesis that COT represents a transient crystalline phase stabilized under specific kinetic conditions.

Furthermore, the solution chemistry, specifically pH and ionic strength, played a decisive role in directing the system toward COT. Our data indicate that a pH exceeding 6.36 invariably leads to the precipitation of COT, which complements the reports by Manissorn *et al.* regarding the efficiency of COM crystallization at lower pH values (pH 4.0).[46] The observed promotion of COT formation at lower ionic strength (0.01 mol dm^{-3}–0.1 mol dm^{-3}) likely results from reduced electrostatic shielding and enhanced ion–ion interactions, which accelerate nucleation dynamics. This is further supported by the magnetic stirring employed in our study; literature consistently reports that such hydrodynamic conditions promote fast heterogeneous nucleation, favoring COT as the initial dominant phase.[45]

The exclusive formation of pure COT in specific runs (*e.g.*, run 1, 9, and 13) can be interpreted through both modern surface-energy modeling and the local concentration model. According to Debroise *et al.*, the stability of CaOx polyhydrates is governed by hydration-dependent surface energies.[47] At moderate temperatures and high-water activity, COT exposes hydrated crystal faces whose surface energetics are lower than those of dehydrated phases, thus stabilizing the lattice in solution. Morphologically, the plate-like, lamellar crystals observed in our SEM images are typical of this kinetically favored phase. This is further explained by the local concentration model proposed by Wang *et al.*, which suggests that COT preferentially nucleates when local ion concentrations during mixing remain low (<1.25 mM). In our system, the high Ca : Ox molar ratio (5.7 : 1), combined with moderate mixing and low ionic strength, effectively reduced local supersaturation during initial contact, placing the system precisely within the regime where COT is favored over COM or COD.[22]

In summary, the dominance of COT observed in our experiments arises from a synergistic interplay of factors: a temperature-controlled kinetic window, pH-regulated availability of oxalate ions, and surface-energy stabilization, all operating within a local concentration regime that suppresses the transition to more stable calcium oxalate hydrates. The successful preparation of phase-pure COT establishes a well-defined metastable reference system for investigating hydration–dehydration pathways, solvent-mediated phase transformations, and crystallization kinetics in calcium oxalate materials. Its availability enables future studies to systematically probe the factors governing its stability and transformation toward more stable hydrates, with potential implications for biomineralization processes, inhibitor design, and the development of advanced analytical methodologies.

Conclusion

This study demonstrates that the response surface methodology combined with a Box–Behnken experimental design is an effective approach for controlling and optimizing the formation of calcium oxalate hydrates, with particular emphasis on the metastable COT phase. Pure COT formation was found to be governed by a narrow kinetic window defined by moderate temperatures (25–36.5 °C), pH values above 6.36, and low ionic strength.

The optimization strategy identified a robust set of conditions (34.25 °C, pH 7.35, I_c = 0.093 mol dm^{-3}) that consistently yields phase-pure COT, while revealing that significant morphological variability can still occur under closely related conditions.

Overall, this work provides a reproducible experimental framework for the controlled synthesis of COT and contributes to a deeper understanding of the physicochemical factors governing calcium oxalate hydrate formation.

Author contributions

A. H. and N. M. M. performed the synthesis and characterization of the compounds and conducted optical analyses and data interpretation. N. M. M. and A. S. conducted the calculation of initial supersaturation, saturation ratios, and ionic strength using VMINTEQ 3.1 and performed data analysis and interpretation. I. S. and J. B. K. performed SEM analyses and interpretation. A. H., N. M. M., N. F., and J. B. K. analyzed and interpreted the FTIR and PXRD results and prepared the visualizations. M. B. performed the three-factor independent quadratic Box–Behnken design (BBD), including data analysis, interpretation, and visual presentation. A. H., N. M. M., N. F., J. B. K., A. S., and M. B. wrote the original manuscript draft. N. M. M., N. F., J. B. K., A. S., and M. B. prepared the revised version of the manuscript. A. S. conceived the project and supervised and guided the experimental design, data analysis, and interpretation and contributed to methodology development, supervision, project administration, and funding acquisition. All authors have read and agreed to the published version of the manuscript.

Conflicts of interest

The authors declare no conflicts of interest.

Data availability

The data supporting the findings of this study are included within the article and its supplementary information (SI).

Supplementary information is available. See DOI: https://doi.org/10.1039/d6ce00201c.

Acknowledgements

This research was funded by the European Union-NextGenerationEU Project "Advanced Interdisciplinary Approaches to Environmental Chemistry: From Materials to Sustainable Solutions for Pollution" (Grant number: 581-UNIOS-101). We thank Professor B. Marković and Professor Á. Kukovecz for their expert advice on data interpretation and for facilitating the international cooperation that made this work possible.

References

1 A. Arnold, E. Dennison, C. S. Kovach, M. Mannstadt, R. Rizzoli, M. L. Brandi, B. Clarke and R. V. Thakker, Hormonal Regulation of Biomineralization, *Nat. Rev. Endocrinol.*, 2021, **17**, 261–275, DOI: 10.1038/s41574-021-00477-2.

2 S. Weiner and P. M. Dove, An Overview of Biomineralization Processes and the Problem of the Vital Effect, *Rev. Mineral. Geochem.*, 2023, **54**(1), 1–29, DOI: 10.2113/0540001.

3 A. L. Boskey, Biomineralization: Conflicts, Challenges, and Opportunities, *J. Cell. Biochem.*, 1998, **72**, 83–91, DOI: 10.1002/(SICI)1097-4644(1998)72:30/31+<83::AID-JCB12>3.0.CO;2-F.

4 N. Vidavsky, J. A. M. R. Kunitake and L. A. Estroff, Multiple Pathways for Pathological Calcification in the Human Body, *Adv. Healthcare Mater.*, 2021, **10**(4), 2001271, DOI: 10.1002/adhm.202001271.

5 M. A. Fuery, L. Liang, F. S. Kaplan and E. R. Mohler, Vascular Ossification: Pathology, Mechanisms, and Clinical Implications, *Bone*, 2018, **110**, 28–34, DOI: 10.1016/j.bone.2017.07.006.

6 A. L. Durham, M. Y. Speer, M. Scatena, C. M. Giachelli and C. M. Shanahan, Role of Smooth Muscle Cells in Vascular Calcification: Implications in Atherosclerosis and Arterial Stiffness, *Cardiovasc. Res.*, 2018, **114**(4), 590–600, DOI: 10.1093/cvr/cvy010.

7 S. R. Khan, M. S. Pearle, W. G. Robertson, G. Gambaro, B. K. Canales, S. Doizi, O. Traxer and H. G. Tiselius, Kidney Stones, *Nat. Rev. Dis. Primers*, 2016, **2**, 16008, DOI: 10.1038/nrdp.2016.8.

8 C. Y. Pak, Kidney Stones, *Lancet*, 1998, **351**(9118), 1797–1801, DOI: 10.1016/S0140-6736(98)01295-1.

9 T. Chen, B. Qian, J. Zou, P. Luo, J. Zou, W. Li, Q. Chen and L. Zheng, Oxalate as a Potent Promoter of Kidney Stone Formation, *Front. Med.*, 2023, **10**, 1159616, DOI: 10.3389/fmed.2023.1159616.

10 V. Y. Bird and S. R. Khan, How Do Stones Form? Is Unification of Theories on Stone Formation Possible?, *Arch. Esp. Urol.*, 2017, **70**(1), 12–27, PMID: 28221139.

11 R. Nazarian, N. Lin, S. Thaker, R. Yang, G. C. L. Wong and K. B. Scotland, What Causes Calcium Oxalate Kidney Stones to Form? An Update on Recent Advances, *Uro*, 2025, **5**(1), 6, DOI: 10.3390/uro5010006.

12 *The Kidney*, ed. B. M. Brenner and F. C. Rector, WB Saunders, Philadelphia, 1976, vol. 1.

13 V. Romero, H. Akpinar and D. G. Assimos, Kidney Stones: A Global Picture of Prevalence, Incidence, and Associated Risk Factors, *Rev. Urol.*, 2010, **12**(2–3), 86–96, PMID: 20811557.

14 X. Y. Sun, C. Y. Zhang, P. Bhadja and J. M. Ouyang, Preparation, Properties, Formation Mechanisms and Cytotoxicity of Calcium Oxalate Monohydrate with Various Morphologies, *CrystEngComm*, 2018, **20**, 75–87, DOI: 10.1039/C7CE01912B.

15 M. Daudon, A. Dessombz, V. Frochot, E. Letavernier, J. P. Haymann, P. Jungers and D. Bazin, Comprehensive Morpho-Constitutional Analysis of Urinary Stones Improves Etiological Diagnosis and Therapeutic Strategy of Nephrolithiasis, *C. R. Chim.*, 2016, **19**, 1470–1491, DOI: 10.1016/j.crci.2016.05.008.

16 M. Daudon, R. J. Réveillaud and P. Jungers, Piridoxilate-Associated Calcium Oxalate Urinary Calculi: A New Metabolic Drug-Induced Nephrolithiasis, *Lancet*, 1985, **1**(8441), 1338, DOI: 10.1016/S0140-6736(85)92835-1.

17 M. Daudon, R. J. Reveillaud, M. Normand, C. Petit and P. Jungers, Piridoxilate-Induced Calcium Oxalate Calculi: A New Drug-Induced Metabolic Nephrolithiasis, *J. Urol.*, 1987, **138**(2), 258–261, DOI: 10.1016/S0022-5347(17)43111-9.

18 G. J. Gardner, Nucleation and Crystal Growth of Calcium Oxalate Trihydrate, *J. Cryst. Growth*, 1975, **30**(2), 158–168, DOI: 10.1016/0022-0248(75)90085-8.

19 M. Daudon, C. A. Bader and P. Jungers, Urinary Calculi: Review of Classification Methods and Correlations with Etiology, *Scanning Microsc.*, 1993, **7**(3), 1081–1104, PMID: 8146609.

20 H. Werner, S. Bapat, M. Schobesberger, D. Segets and S. P. Schwaminger, Calcium Oxalate Crystallization: Influence of pH, Energy Input and Supersaturation Ratio on the Synthesis of Artificial Kidney Stones, *ACS Omega*, 2021, **6**(40), 26566–26574, DOI: 10.1021/acsomega.1c03938.

21 M. Yuzawa, K. Tozuka and A. Tokue, Effect of Citrate and Pyrophosphate on the Stability of Calcium Oxalate Dihydrate, *Urol. Res.*, 1998, **26**(2), 83–88, DOI: 10.1007/s002400050028.

22 Z. Wang, L. Du, Q. Wang, J. Xie, Z. Fu and Z. Zou, Local Concentration Controls the Hydrate Phase of Calcium Oxalate, *CrystEngComm*, 2024, **26**, 2394–2403, DOI: 10.1039/D3CE01286G.

23 J. Dietrich, A. Costa-Bauza and F. Grases, Thermodynamic and Kinetic Aspects of Calcium Oxalate Crystallization and Renal Lithiasis, *Biomolecules*, 2025, **15**(8), 1141, DOI: 10.3390/biom15081141.

24 D. Kim, V. P. Chauhan, B. G. Alamani, S. D. Fisher, Z. Yang, M. R. Jones, T. Terlier, P. G. Vekilov and J. D. Rimer, Bio-Inspired Multifunctional Disruptors of Calcium Oxalate Crystallization, *Nat. Commun.*, 2025, **16**, 60320, DOI: 10.1038/s41467-025-60320-4.

25 A. R. Izatulina, V. V. Gurzhiy, M. Krzhizhanovskaya, M. A. Kuz'Mina, M. Leoni and O. V. Frank-Kamenetskaya, Hydrated Calcium Oxalates: Crystal Structures, Thermal Stability and Phase Evolution, *Cryst. Growth Des.*, 2018, **18**, 5465–5478, DOI: 10.1021/acs.cgd.8b00826.

26 C. Berg and H. G. Tiselius, The Effect of pH on the Risk of Calcium Oxalate Crystallization in Urine, *Eur. Urol.*, 1986, **12**(1), 59–61, DOI: 10.1159/000472578.
27 U. Michibata, M. Maruyama and Y. Tanaka, *et al.*, Impact of Crystal Phase Transition on the Hardness and Structure of Kidney Stones, *Urolithiasis*, 2024, **52**(1), 57, DOI: 10.1007/s00240-024-01556-5.
28 I. H. Valido, J. M. Ruis-Bartra, R. Boada, M. Resina-Gallego, M. Valiente and M. Lopez-Mesas, Characterization of Calcium Oxalate Hydrates and the Transformation Process, *ChemPhysChem*, 2020, **21**(22), 2583–2593, DOI: 10.1002/cphc.202000684.
29 A. Šter, S. Šafranko, K. Bilić, B. Marković and D. Kralj, Effect of Hydrodynamic and Thermodynamic Factors and Citric Acid Addition on Calcium Oxalate Dihydrate Precipitation, *Urolithiasis*, 2018, **46**(3), 243–256, DOI: 10.1007/s00240-017-0991-0.
30 A. Stanković, S. Šafranko and K. Jurišić, *et al.*, Investigation of System Complexity and Vitamin C on Calcium Oxalate Precipitation, *Chem. Pap.*, 2020, **74**(10), 3279–3291, DOI: 10.1007/s11696-020-01157-7.
31 A. Stanković, S. Šafranko, J. Kontrec, B. Njegić-Džakula, D. M. Lyons, B. Marković and D. Kralj, Calcium Oxalate Precipitation in Model Systems Mimicking Hyperoxaluria, *Cryst. Res. Technol.*, 2019, **54**(6), e1800210, DOI: 10.1002/crat.201800210.
32 S. Šafranko, S. Goman and D. Goman, *et al.*, Calcium Oxalate and Gallic Acid: Structural Characterization and Process Optimization Toward Obtaining High COM and COD Contents, *Crystals*, 2021, **11**(8), 954, DOI: 10.3390/cryst11080954.
33 A. Stanković, N. Matijaković Mlinarić, J. Kontrec, B. Njegić-Džakula, D. M. Lyons, B. Marković and D. Kralj, Influence of Amino Acids on Calcium Oxalate Precipitation in Systems of Different Chemical Complexity, *Crystals*, 2024, **14**(7), 599, DOI: 10.3390/cryst14070599.
34 C. Conti, M. Casati and C. Colombo, *et al.*, Synthesis of Calcium Oxalate Trihydrate: New Data by Vibrational Spectroscopy and Synchrotron X-Ray Diffraction, *Spectrochim. Acta, Part A*, 2015, **150**, 721–730, DOI: 10.1016/j.saa.2015.06.009.
35 Z. Chen, C. Wang, H. Zhou, L. Sang and X. Li, Modulation of Calcium Oxalate Crystallization by Green Tea, *CrystEngComm*, 2010, **12**, 845–852, DOI: 10.1039/B913589H.
36 I. Petit, G. D. Belletti and T. Debroise, *et al.*, Vibrational Signatures of Calcium Oxalate Polyhydrates, *ChemistrySelect*, 2018, **3**(31), 8801–8812, DOI: 10.1002/slct.201801611.
37 J. M. Ouyang, H. Zheng and S. P. Deng, Simultaneous Formation of Calcium Oxalate Hydrates Induced by Potassium Tartrate, *J. Cryst. Growth*, 2006, **293**(1), 118–123, DOI: 10.1016/j.jcrysgro.2006.05.008.
38 M. Ben Cheikh, N. Kamoun, A. Boulila and S. Ammar, Calcium Oxalate Trihydrate: Vibrational Spectroscopy and Synchrotron X-Ray Diffraction, *Spectrochim. Acta, Part A*, 2015, **150**, 581–588, DOI: 10.1016/j.saa.2015.06.009.
39 C. P. East, A. Wallace, A. Al-Hamzah, W. O. S. Doherty and C. M. Fellows, Effect of Poly(acrylic Acid) Molecular Mass and End-Group Functionality on Calcium Oxalate Crystal Growth, *J. Appl. Polym. Sci.*, 2010, **115**(4), 2127–2135, DOI: 10.1002/app.31342.
40 B. B. Tomazic and G. H. Nancollas, Calcium Oxalate Hydrates: Dissolution, Transformation and Crystallization Studies, in *Urolithiasis: Clinical and Basic Research*, ed. P. E. N. Ransley and J. J. Feeley, Springer, 1990, pp. 453–457.
41 A. Thomas, P. Simon, W. Carrillo-Cabrera and E. Sturm, Biomimetic Growth of Calcium Oxalate Hydrates, *Chem. – Eur. J.*, 2025, **31**(25), e202404269, DOI: 10.1002/chem.202404269.
42 J. M. Ouyang, Effects of Temperature on Calcium Oxalate Growth in Silica Gels Containing Carboxylic Acids, *Mater. Sci. Eng., C*, 2006, **26**(4), 679–682, DOI: 10.1016/j.msec.2005.06.060.
43 J. Ouyang, S. Deng, X. Li, Y. Tan and B. Tieke, Temperature and Sodium Carboxylate Effects on Calcium Oxalate Mineralization, *Sci. China, Ser. B: Chem.*, 2004, **47**(4), 311–319.
44 L. Brečević and D. Kralj, Factors Influencing Calcium Oxalate Hydrate Formation In Vitro, *Med. Vjesn.*, 2010, **42**(3–4), 127–136, https://hrcak.srce.hr/191918.
45 D. Škrtić, H. Furedi-Milhofer and M. Marković, Calcium Oxalate Precipitation from High Ionic Strength Solutions, *J. Cryst. Growth*, 1987, **80**, 113–120, DOI: 10.1016/0022-0248(87)90530-6.
46 J. Manissorn, K. Fong-Ngern, P. Peerapen and V. Thongboonkerd, Urine pH Effects on Calcium Oxalate Crystallization and Cell Interaction, *Sci. Rep.*, 2017, **7**, 1–11, DOI: 10.1038/s41598-017-01953-4.
47 T. Debroise, T. Sedzik, J. Vekeman, Y. Su, C. Bonhomme and F. Tielens, Morphology of Calcium Oxalate Polyhydrates: A Quantum Chemical Study, *Cryst. Growth Des.*, 2020, **20**(6), 3807–3815, DOI: 10.1021/acs.cgd.0c00119.